Nuclear Engineering and Technology 58 (2026) 104165

Contents lists available at ScienceDirect

Nuclear Engineering and Technology

journal homepage: www.elsevier.com/locate/net

Original Article

Mineralization and radioactive potential of Magal Gebreel rocks, South Eastern Desert, Egypt: Health risk evaluation

Gehad M. Saleh [a], Basma A. El-Badry [b], Mabrouk Sami [c], Tamader Alhazani [b], Omnia T. Amer [a], Ioan V. Sanislav [d], El Saeed R. Lasheen [e,*]

[a] Nuclear Materials Authority, P. O. Box 530, El-Maadi, Cairo, Egypt
[b] Physics Department, Faculty of Science, Imam Mohammad Ibn Saud Islamic University (IMSIU), Riyadh, Saudi Arabia
[c] Geosciences Department College of Science United Arab Emirates University, 15551, Al Ain, United Arab Emirates
[d] Economic Geology Research Centre (EGRU), College of Science and Engineering, James Cook University, Townsville, QLD, 4811, Australia
[e] Geology Department, Faculty of Science, Al-Azhar University, Cairo, 11884, Egypt

ARTICLE INFO

Keywords:
Radiological hazards
Radioactive content
Granitic phases
Magal Gebreel rocks mineralization

ABSTRACT

The present research aims to evaluate the radiation dosages in the Magal Gebreel granitic phases, which encompass monzogranites, alkali feldspar granites, and altered granites (widely exposed along the shear zone). The former rocks have an average of 89.28 ± 23.85 Bqkg^{-1} for ^{238}U, 51.71 ± 9.65 Bqkg^{-1} for ^{232}Th, and 995.34 ± 160.21 Bqkg^{-1} for 40K utilizing the NaI (Tl) analyzer. Alkali feldspar granites have an average of 146.32 ± 46.73 Bqkg^{-1} for ^{238}U, 77.57 ± 11.21 Bqkg^{-1} for ^{232}Th, and 1120.54 ± 26 Bqkg^{-1} for ^{40}K. The later (altered granites) have the highest activity concentrations of ^{232}Th (avg. 360.57 ± 58.02 Bqkg^{-1}), ^{40}K (avg. 1197.23 ± 106.53 Bqkg^{-1}), and ^{238}U (avg. 3797.50 ± 725.68 Bqkg^{-1}), as well as their summation (avg. 2201.60 ± 250.62 Bqkg^{-1}). It is obvious that the investigated rocks contain increased activity concentrations and therefore fall above the widely accepted worldwide requirements. The results of microscopic and ESEM analysis revealed large assemblages of significant minerals enclosed in the Magal Gebreel rocks such as precious, base metals, accessories, radioactive-bearing, REE-bearing, and Nb-Ta- bearing minerals. Radium equivalent, dose of human body, absorbed dose rate and annualized dosage, excess life-time cancer, coupled with extra radiological characteristics were inferred for these rocks. Given that the measures of most of these criteria are higher than the international average, it is distinct that the tested rocks (certainly altered granites) have a considerable effect on the natural gamma emission released.

1. Introduction

The crust of the Earth has a dynamic repository of natural radionuclides that have existed since the creation of the planet, where the terrestrial (^{232}Th, ^{238}U, and ^{40}K) radionuclides are abundant [1–3]. Long-term processes are unaffected by the presence of radium due to its continual generation and comparatively short half-life, which is produced by the decay of ^{232}Th and ^{238}U and ^{235}U [4,5]. Variable rocks have different levels of mobility, the disequilibrium between uranium and radium happens periodically [6]. Radionuclide concentrations are important for monitoring environmental radioactivity, considering the geographical variation in the external gamma dose rate. These dosages are determined by the amounts of radionuclides that naturally exist in rocks [7,8]. Deposition, erosion, and weathering are common mechanisms that preferentially enhance radionuclides, particularly in the late stages of granitic rocks. For example, uranium has been seen to interact with biological matter and phosphate minerals [9–11]. This geological separation results in the formation of distinct high-radiation zones, which may remain inactive until affected by natural erosion or human activities such as mining or hydraulic fracturing. The interrelationship of sedimentary rock lithology and motion of radionuclides emphasizes the difficulty in anticipating and explaining the associated dangers [3,12,13,13,14]. Recently, there is a focus on tracking the natural distribution of radioactive elements. Numerous study endeavors have been launched everywhere to ascertain the total radiation dosage of the rocks [2,4,12,15–21].

Recent studies indicate that environments with elevated ^{238}U and ^{226}Ra concentrations frequently show increased radon flux, which can

* Corresponding author.
E-mail address: elsaeedlasheen@azhar.edu.eg (E.S.R. Lasheen).

https://doi.org/10.1016/j.net.2026.104165
Received 15 October 2025; Received in revised form 19 January 2026; Accepted 24 January 2026
Available online 29 January 2026

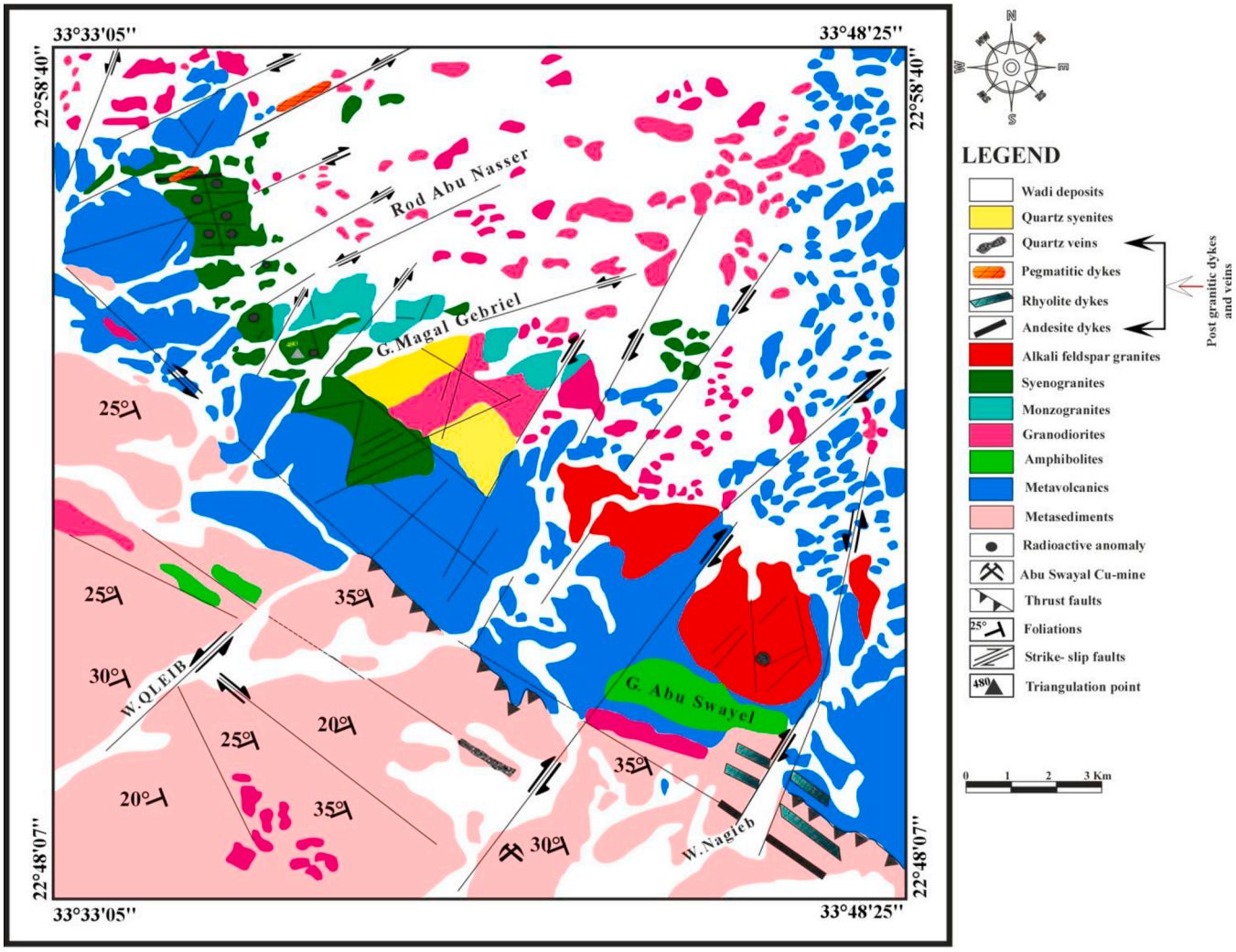

Fig. 1. Magal Gebreel geologic map, South Eastern Desert, Egypt [25].

affect indoor and outdoor radon exposure levels (e.g., UNSCEAR, 2000). Radon emanation and transport are influenced by factors such as porosity, grain size, fracture density, and soil moisture content, all of which can be significant in granitic terrains with high natural uranium content. These granites elevated levels of ^{226}Ra in construction presents a potential radon hazard. This material exhales radon gas, a radioactive byproduct of ^{226}Ra decay, which can lead to excessive concentrations indoors. Radon, which is colorless and odorless, tends to accumulate in areas with inadequate ventilation, such as building basements and ground floors [22–24].

Lasheen [25] conducted one of the few bulk-rock geochemical studies on the Magal Gebreel granitic rocks to elucidate their petrogenesis and emplacement setting. These granites were classified as syn-to post-collisional in origin. The former varieties are granodioritic in composition with calcic to calc-alkaline and magnesian affinities. In contrast, the post-collisional granites correspond to A2-type granites, characterized by low Mg# and Ti contents, coupled with high SiO_2 and Nb.

Granitic rocks are highly evolved lithologies that commonly contain accessory minerals capable of trapping U and Th radioactive elements. Owing to the widespread occurrence of granitic rocks and their extensive use as decorative stones and in various industrial applications, assessing their radioactive characteristics is necessary. This study represents the first radiological evaluation of these granitic rocks, providing essential data for both environmental safety and sustainable utilization.

The goal of this investigation is to pinpoint rock units using the fieldwork and petrography. Besides, we plan to assess the radioactive possibility of the Magal Gebreel rocks. This form of inspection demands determining the delivered radiation doses (^{232}Th, ^{238}U, and ^{40}K) present in these rocks and linking the observed radiological characteristics to mineralogical composition and hydrothermal alteration processes. Moreover, several radiological risk factors have been devised to permit an improved assessment of the negative consequences of radiation on human beings.

2. Field geology

The Neoproterozoic rocks typically occur in the Nubian Shield's (NS) Eastern Desert. These rocks cover the Arabian Peninsula and a portion of Africa, developing the Arabian Nubian Shield and accounting for a ten percent of Egypt's surface area [26]. They encompasses variety of rocks like migmatite, ophiolites, arc-related rocks, phases of granitic rocks, and younger ultramafic intrusion. On top of that, the majority of these rocks have survived mineralization; they can be used for building portions in cement and as stones for decoration since of their attractive forms and extreme durability [27,28]. Granite is the most prevalent rock that exists in the Earth's crust, comprising 60 % of the Nubian Shield [29].

The highly fractionated kind of these rocks are particularly enclosing economic elements (e.g. Au, Li, Nb, B, Ce, Be, Ta, Sn, Y, Ag, Zr, and

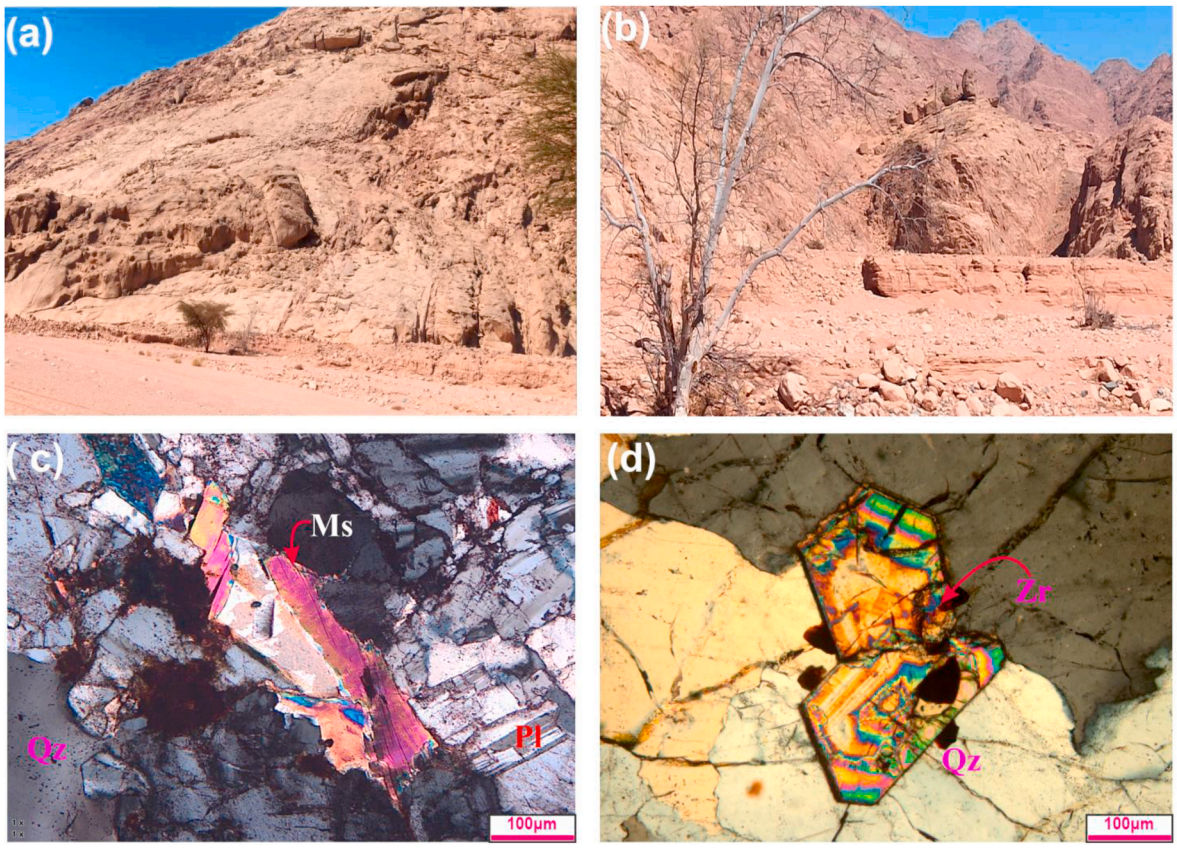

Fig. 2. Field and microscopic photos exhibit: **a)** Smooth surface and cavernous as weathering products; **b**) Large onion shaped granites along shear zones; **c**) Muscovite (Ms) flaks surrounded by plagioclase (Pl) and quartz (Qz); **and d)** Euhedral zircon (Zr) crystals occurred as aggregates within quartz.

REEs) [26,30–33]. The Gabal Magal Gebreel region, a part of the NS, sits in the southern region of Egypt's Eastern Desert (Fig. 1). The highest points are Gabal Magal Gebreel (490 m) and Abu Swayel (375 m) above sea level. This area of study has a variety of igneous and metamorphic rocks, including metasediments, metavolcanics, younger and older granites, plus dykes. Numerous granitic phases are widely exposed. The older granitoids appear on the northern and far eastern portions of this area. They inject metasediments and metavolcanics. In contrast, the younger granites comprise intermediate to elevated topography and cover around 95 km^2. These rocks are widely jointed, cavernous, and have a bouldery morphology (Fig. 2a–b). Field research demonstrated that hydrothermal action affects these granites, particularly near shear zones, triggering hematitization, chloritization, and silicification areas.

3. Methodology

Fourteen samples weighing almost 400 g were collected from the Magal Gebreel rocks and checked with the NaI (Tl) analyzer at the Nuclear Material Authority (supplementary material). Before these samples were put in 200 ml plastic containers, they were air-dried and sieved via a mesh size of around 200. A Bicron scintillating sensor, a 76 × 76 mm NaI (Tl) crystal, and a tube with a photomultiplier enclosed in an aluminum housing constitute the gamma ray. To estimate the radiological implications of samples, implement the following formulas: radium equivalent (Raeq), organs of human dose ($D_{organ\ out\ \&in}$), excess life-time cancer (ELCR), rate of absorbed dose (D_{air}), annualized dosage ($AED_{out\ \&\ in}$), and additional factors (e.g., internal and external indicators; H_{ex} & H_{in}). ^{40}K, ^{238}U, and ^{232}Th activities are denoted by the terms H_K, H_U, and H_{Th}, respectively [34,35,35,35,35,35,36].

$$D_{air}\ (nGyh^{-1}) = 0.430H_U + 0.666H_{Th} + 0.042H_K \quad \text{(eq. 1)}$$

$$Ra_{eq}\ (Bqkg^{-1}) = H_U + 1.43H_{Th} + 0.077H_K \quad \text{(eq. 2)}$$

$$AED\ (mSv/y) = D_{air}\ (nGyh^{-1}) \times 8.76h \times 0.8 \times 0.7 \times 10^{-3} \quad \text{(eq. 3)}$$

where, The occupancy number compensates for occupancy time in cases when outdoor is 0.2 and indoor is 0.8 [34,37].

$$D_{organs} = D_{organs\ in}\ (mSv/y) = AED_{in} \times F \quad \text{(eq. 4)}$$

$$D_{organs\ out}\ (mSv/y) = AED_{out} \times F \quad \text{(eq. 5)}$$

$$H_{ex} = H_U/370 + H_{Th}/259 + H_K/4810 \quad \text{(eq. 6)}$$

$$H_{in} = H_U/185 \text{ for indoor} + H_{Th}/259 + H_K/4810 \quad \text{(eq. 7)}$$

$$ELCR_{in} = AED \times DL\ (70y) \times RF\ (0.05\ S/v) \quad \text{(eq. 8)}$$

4. Results

4.1. Petrography

Mineral and textural characteristics are available for monzogranites, alkali feldspar granites, and altered granites. Medium-grained monzogranites are observed, which contain orthoclase perthite, quartz, and plagioclase, with little muscovite and biotite. Orthoclase perthite ranges from subhedral to anhedral, which are mostly supplanted by sericite and kaolinite. Quartz is anhedral to interstitial grains and particularly associated with perthite. Plagioclase is frequently observed as subhedral crystals. They have slightly transformed toward saussurite. Sericitized muscovite is primarily linked to the development of subhedral fibers alternating with quartz and plagioclase. Alkali feldspar granites are hypidiomorphic and primarily constitute potash feldspar, quartz, plagioclase, and muscovite. Muscovite is found in trace quantities

Table 1
^{40}K, ^{238}U, and ^{232}Th concentrations and their ratios of Magal Gebreel rocks.

Rocks	Samples	^{232}Th (Bqkg^{-1})	^{238}U (Bqkg^{-1})	^{40}K (Bqkg^{-1})	$^{232}Th/^{40}K$	$^{232}Th/^{238}U$
Monzogranites	**MG1**	44.44	74.40	751.20	0.06	0.60
	MG2	52.52	86.80	1189.40	0.04	0.61
	MG3	56.56	124.00	1001.60	0.06	0.46
	MG4	64.64	99.20	1064.20	0.06	0.65
	MG5	40.40	62.00	970.30	0.04	0.65
	Min.	40.40	62.00	751.20	0.04	0.46
	Max.	64.64	124.00	1189.40	0.06	0.65
	Avg.	51.71	89.28	995.34	0.05	0.59
	SD	9.65	23.85	160.21	0.01	0.08
	25 %	44.44	74.4	970.3		
	50 %	52.52	86.8	1001.6		
	75 %	56.56	99.2	1064.2		
Alkali feldspar granites	**MG6**	60.60	74.40	1095.50	0.06	0.81
	MG7	72.72	198.40	1126.80	0.06	0.37
	MG8	80.80	173.60	1158.10	0.07	0.47
	MG9	88.88	148.80	1126.80	0.08	0.60
	MG10	84.84	136.40	1095.50	0.08	0.62
	Min.	60.60	74.40	1095.50	0.06	0.37
	Max.	88.88	198.40	1158.10	0.08	0.81
	Avg.	77.57	146.32	1120.54	0.07	0.57
	SD	11.21	46.73	26.19	0.01	0.17
	25 %	72.72	136.4	1095.5		
	50 %	80.8	148.8	1126.8		
	75 %	84.84	173.6	1126.8		
Altered granites	**MG11**	339.36	3658.00	1158.10	0.29	0.09
	MG12	387.84	3794.40	1095.50	0.35	0.10
	MG13	290.88	2988.40	1345.90	0.22	0.10
	MG14	424.20	4749.20	1189.40	0.36	0.09
	Min.	290.88	2988.40	1095.50	0.22	0.09
	Max.	424.20	4749.20	1345.90	0.36	0.10
	Avg.	360.57	3797.50	1197.23	0.30	0.10
	SD	58.02	725.68	106.53	0.07	0.01
	25 %	327.24	3490.6	1142.45		
	50 %	363.6	3726.2	1173.75		
	75 %	396.93	4033.1	1228.525		

Table 2
Comparison of ^{238}U, ^{40}K, and ^{232}Th concentrations of the Magal Gebreel rocks.

Location	^{238}U (Bqkg^{-1})	^{226}Th (Bqkg^{-1})	^{40}K (Bqkg^{-1})	Reference
Egypt	137.00	82.00	1082.00	[47]
Serbia	200	77	1280	[53]
Saudi Arabia	28.82	34.83	665.08	[16]
Sharm El Luli, Egypt	24.57	23.32	241.83	[8]
Abu Ghusun coastline	24.53	12.1	337.06	[46]
Jeddah shoreline	13.14	5.05	139.09	[2]
Wadi El Gemal Island	12.49	12.63	325.13	[17]
India	25.88	42.82	560.60	[48]
Spain	84	42	1138	[49]
Egypt	137	82	1082	[54]
Egypt	1674	105.04	683.91	[50]
Egypt	175	92.25	899.2	[55]
Granit S Tropez, Italy	101 ± 9	167 ± 17	1230 ± 40	[24]
Granite, China	98 ± 3	119 ± 4	1290 ± 70	[24]
Granite block, Italy	110 ± 7	106 ± 9	1330 ± 160	[24]
Rosso, Italy	160 ± 10	160 ± 15	1300 ± 110	[24]
New Kristal, Croatia	102 ± 6	77 ± 4	1180 ± 70	[24]
EU, Granit Rosa Por	280 ± 40	81 ± 14	1060 ± 80	[24]
Monzogranites	89.28	51.71	995.34	Current study
Alkali feldspar granites	146.32	77.57	1120.54	
Altered granites	3797.50	360.57	1197.23	

(Fig. 2c). Quartz is the most common component. Plagioclase occurs as tabular crystals with morphologies ranging from euhedral to subhedral and exhibiting stunning lamellar twinning. Almost all of them are still fresh; however, some are slightly saussuritized. Some samples show the presence of a flake of biotite. The medium-sized Magal Gebreel altered granites are mostly made up of flamy perthite, plagioclase, and quartz. The former is found as platy crystals, which are frequently fully kaolinitized and broken. Plagioclase develops to form subhedral with a lack of twinning due to the alteration role. Both the initial and secondary generations of muscovite are present. The observed accessories include allanite, uranophane, and zircon. Zoned zircon is a euhedral crystal that can be found at the edges of quartz (Fig. 2d).

4.2. Radionuclides abundance

The occurrence and percentages of radioactive elements ^{40}K, ^{232}Th, and ^{238}U have been established for fourteen samples obtained from the Magal Gebreel rocks (Table 1). The median ± SD results for ^{40}K, ^{232}Th, and ^{238}U in less evolved granitic rocks (monzogranites) are 995.34 ± 160.21 Bqkg^{-1}, 51.71 ± 9.65 Bqkg^{-1}, 89.28 ± 23.85 Bqkg^{-1}, respectively. Alternatively, ^{40}K are between 1095.50 and 1158.10 Bqkg^{-1}, ^{238}U between 74.40 and 198.40 Bqkg^{-1}, and ^{232}Th ranged from 60.60 to 88.88 Bqkg^{-1} in alkali feldspar granites. It is obvious from the correlation with monzogranites and alkali feldspar granites, the evaluated altered granites from the Magal Gebreel area has the greatest acquired activity concentrations of ^{40}K (avg. 1197.23 ± 106.53 Bqkg^{-1}), ^{238}U (avg. 3797.50 ± 725.68 Bqkg^{-1}), ^{232}Th (avg. 360.57 ± 58.02 Bqkg^{-1}), and their combination (avg. 2201.60 ± 250.62 Bqkg^{-1}) (Table 1). This is due to the presence of zircon, kasolite, uranophane, and thorite, which integrate radionuclide into their structures. Moreover, the extremely high ^{238}U concentrations in the altered granites can be attributed to

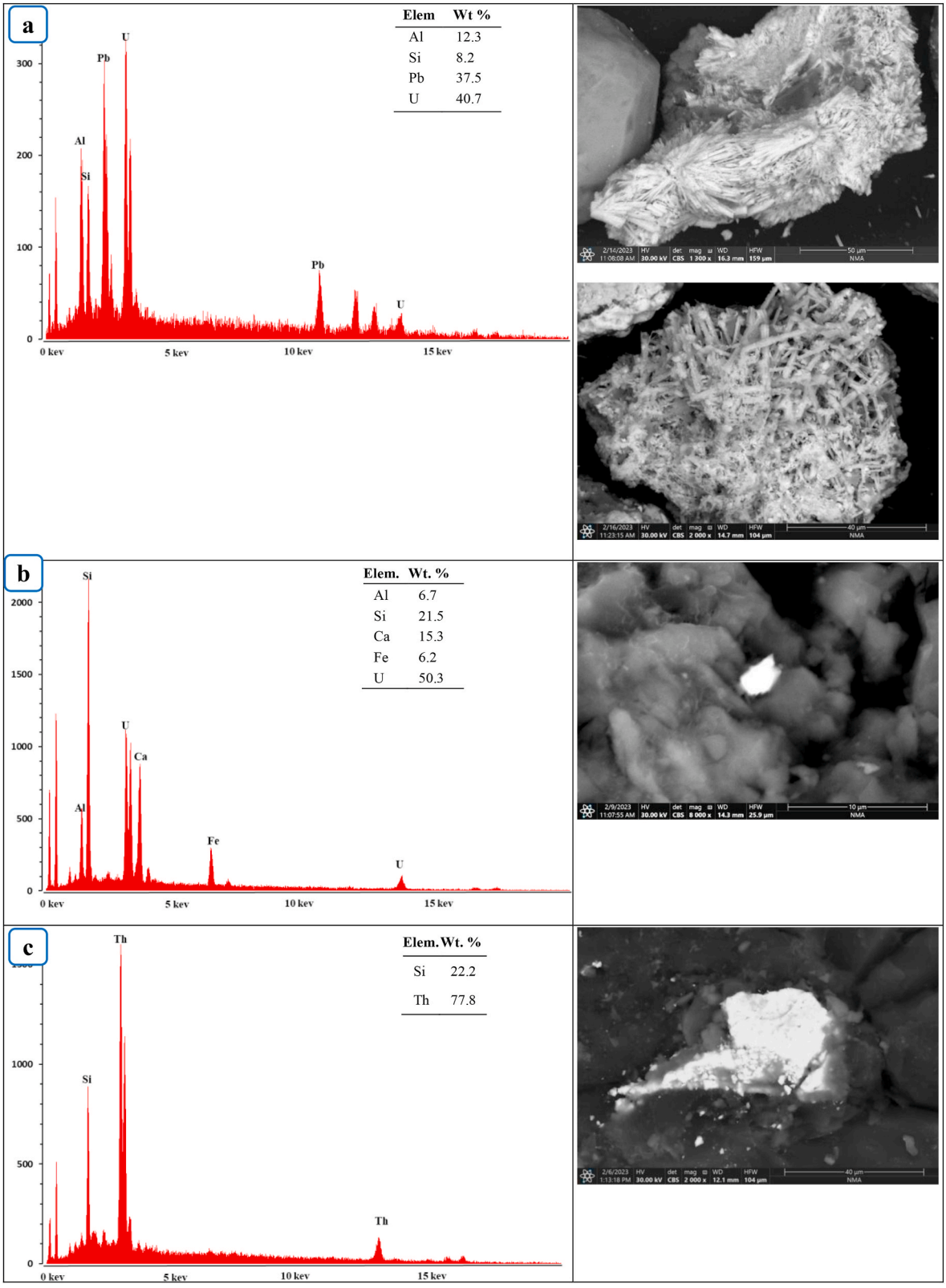

Fig. 3. BSE images and EDX patterns of: **a**) Kasolite, **b**) Uranophane, and **c**) Thorite mineral.

several interrelated geological processes. Hydrothermal alteration played a primary role by mobilizing uranium from the original granitic matrix and redepositing it along fractures, shear zones, and altered domains, where fluid-rock interaction was intense. Metasomatic processes further enriched uranium through chemical exchange between hydrothermal fluids and the host granites, leading to the concentration of U in specific mineral phases and altered zones. Structural features, including faults and shear zones, enhanced fluid circulation and provided pathways for uranium-bearing fluids, ultimately resulting in localized but exceptionally high U enrichment within the granitic rocks

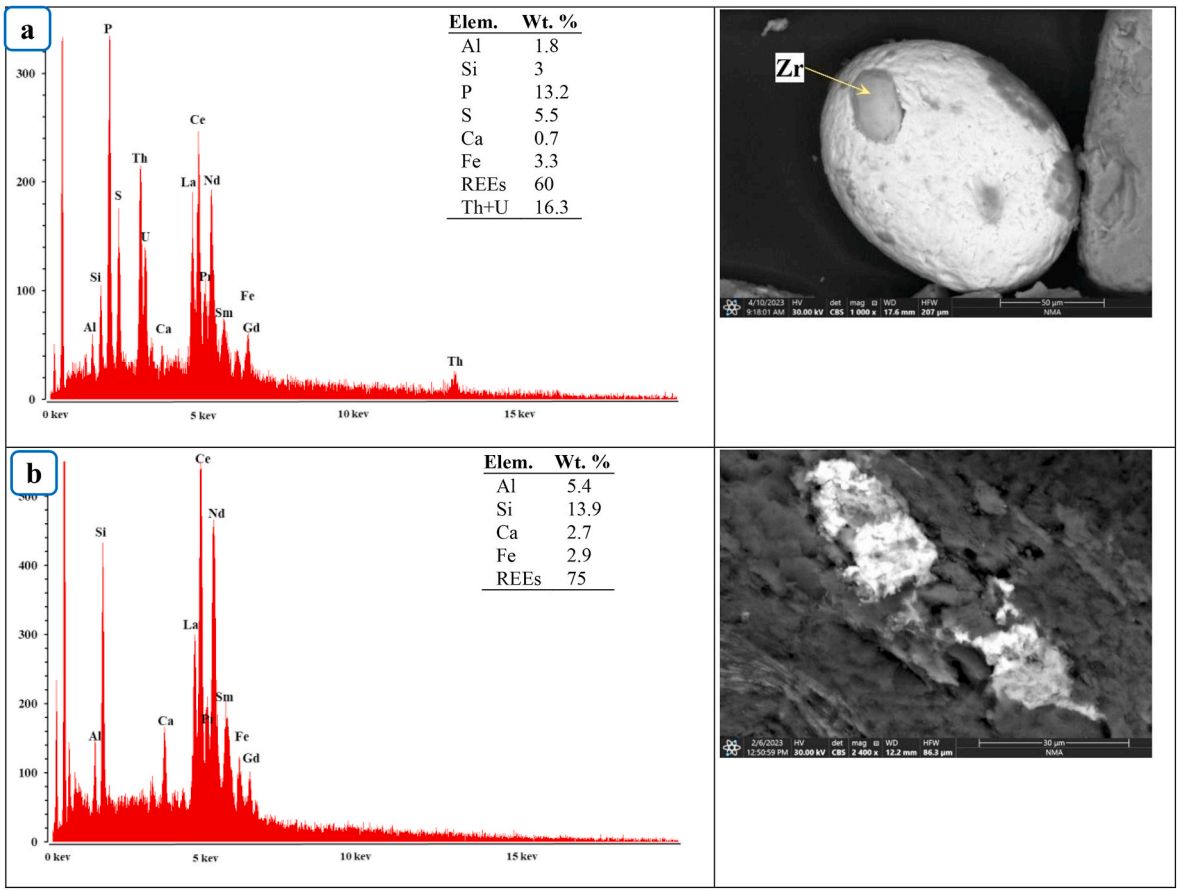

Fig. 4. BSE images and EDX patterns of: **a**) monazite and **b)** allanite mineral.

[2,38,39].

Controversy, the assessed monzogranites the lowest ^{40}K, ^{232}Th, and ^{238}U concentrations when correlated with other rocks. Overall, all the assessed rocks have ^{40}K, ^{232}Th, and ^{238}U radioactive concentration surpass the approved universal standards [12,19,21,35,40–42]. Likewise, following the worldwide recording rules, the activity summing ($^{40}K+ ^{232}Th + ^{238}U$) of all samples surpasses the allowed range of 420 Bq kg^{-1} [20,43].

The altered granites had a minimal $^{232}Th/^{238}U$ ratio (0.1 ± 0.01), lower than the global average of 3.94. The smallest observations are associated with high U levels in comparison to Th in the assessed samples, indicating U migration with regard to Th in the altered granites [44]. This is the result of secondary U increase during subsequent hydrothermal activity [1,13,41,43,45]. Table 1 shows that the altered granites had the greatest $^{232}Th/^{40}K$ (avg. 0.3 ± 0.07), exceeding the universal reporting standard of 0.07). This could be explained by the high potassium concentration of these rocks as a result of K-metasomatism. Actually, the samples collected from the Magal Gebreel area show a sequence of their activity levels shown below: $^{40}K > ^{238}U > ^{232}Th$ (Table 1).

Table 2 shows the findings of currently ongoing analysis (^{40}K, ^{238}U, and ^{232}Th) in contrast to global standards. They surpass the permissible quantity of [35], and others like those of phosphorite [16], Abu Ghusun coastline [46], Jeddah coastline [2], Sharm El Luli coastline [8], Wadi El- Gemal sediments [17], commercial granitic rocks [47], flooring materials [48], Sapin granites [49], and worldwide from Italy, China, and EU [24]. Anyway, the assessed altered granites have ^{238}U akin to rocks of El Missikat altered granites [50]. The U and Th are preferentially incorporated into accessory and radioactive minerals such as zircon, monazite, thorite, kasolite, and uranophane, particularly in altered granitic rocks affected by hydrothermal fluids and metasomatism [1,13,41,43,45]. In contrast, Th activity is mainly governed by the modal proportion of K-bearing rock-forming minerals, especially K-feldspar and biotite [21,39,40,51,52]. Therefore, rocks enriched in accessory U-Th-bearing minerals show elevated U and Th activities, whereas variations in K activity largely reflect differences in the abundance of K-rich feldspars and micas [1,45].

4.3. Mineralization

The results of microscopic examination and ESEM analysis revealed that the rocks of Magal Gebreel have large assemblages of minerals (radioactive, REEs- bearing minerals, Nb-Ta minerals, precious, base metals, and accessories).

A. Radioactive minerals

Kasolite, uranophane, and thorite are the main radioactive minerals identified in the altered Magal Gebreel granites, reflecting the significant role of hydrothermal solutions in their formation.

Kasolite Pb (UO_2) SiO_4. (H_2O) occurs in multiple forms (radial fibers/clusters). It is mostly constituted of U (40.7 wt%), Pb (37.5 wt%), and Si (8.2 wt%) (Fig. 3a). Uranophane (Ca (UO_2) $(SiO_2)_2(OH)_2.5H_2$) is found as minute fiber clusters on the quartz surface, as yellow radials in the voids, and as a coating across joining planes.

The majority of the uranophane detected was coupled with iron oxides (hematite) in the oxidized areas of the rocks and looks to be of supergene provenance. The EDX examination validated its composition: U (50.3 wt%), Ca (15.3 wt%), and Si (21.5 wt%) (Fig. 3b).

Thorite ($ThSiO_4$) appears as tiny tetragonal crystals grouped in a radiating (rose-like) pattern around kasolite cores. The EDX examination established the system's composition as Th (77.8 wt%) and Si (22.2

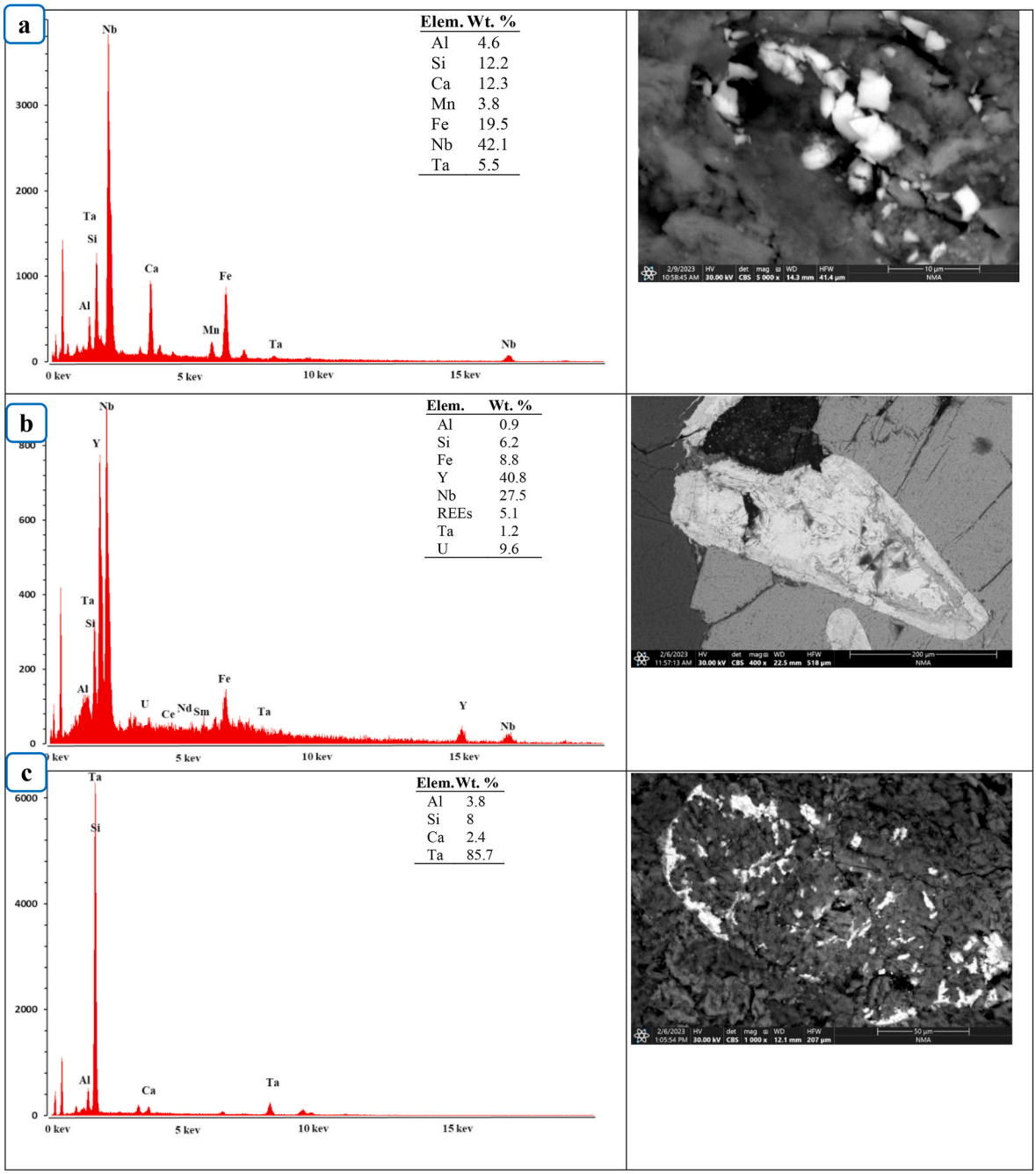

Fig. 5. EDX spectra and BSE image of: **a**) Columbite, **b**) Fergusonite, and **c**) Tantite mineral.

wt%) (Fig. 3c).

B. REEs-bearing minerals

Monazite [(Ce, La, Th, Nd, Y) PO_4] found as rounded crystals enclosing zircon. U might inhabit some of the REE positions in monazite [56]. EDX investigation revealed that it has a high amount of LREEs (60 wt%; particularly Ce) with P (13.2 wt%) and Th + U (16.3 wt%) (Fig. 4a).

Allanite (REEs, Ca,Y)$_2$(Al, Fe^{3+})$_3$(SiO_4)$_3$(OH) belongs to the epidote group, although it is less stable than other members. Almost allanite includes some Th as much as three percent. [57]. The EDX analyses give Ca (2.7 wt %), LREEs (75 wt %) and Al (5.4 wt %) (Fig. 4b).

C. Nb- &Ta-bearing minerals

Columbite- (Fe) is the common Nb-bearing mineral and constitutes a major resource of the technologically valuable metal. Absence of U in the columbite structure may be attributed to decreasing in the temperature of crystallization [58]; indicating hydrothermal solution role in accumulation of the mineral. The analyses show that ferro-columbite is composed mainly of Nb (42 wt %), Ta (5.5 wt %), Fe (19.5 wt %) with traces of Mn (Fig. 5a).

Fergusonite with chemical formula (Y, REE)NbO_4. It exists as an accessory mineral in felsic rocks and is frequently associated with a number of Y, Th, Nb, Ta, and Ti oxide. The ESEM is used to identify this mineral, which contains Nb (27.5 wt%), Y (40.8 wt%), and REEs (5.1 wt %), as well as traces of U (Fig. 5b).

Tantite mineral, a resistant to corrosion metal, is mostly derived from the chemical element Ta_2O_5. It is chemically related to columbite and is frequently classed collectively as a semi-singular mineral termed coltan

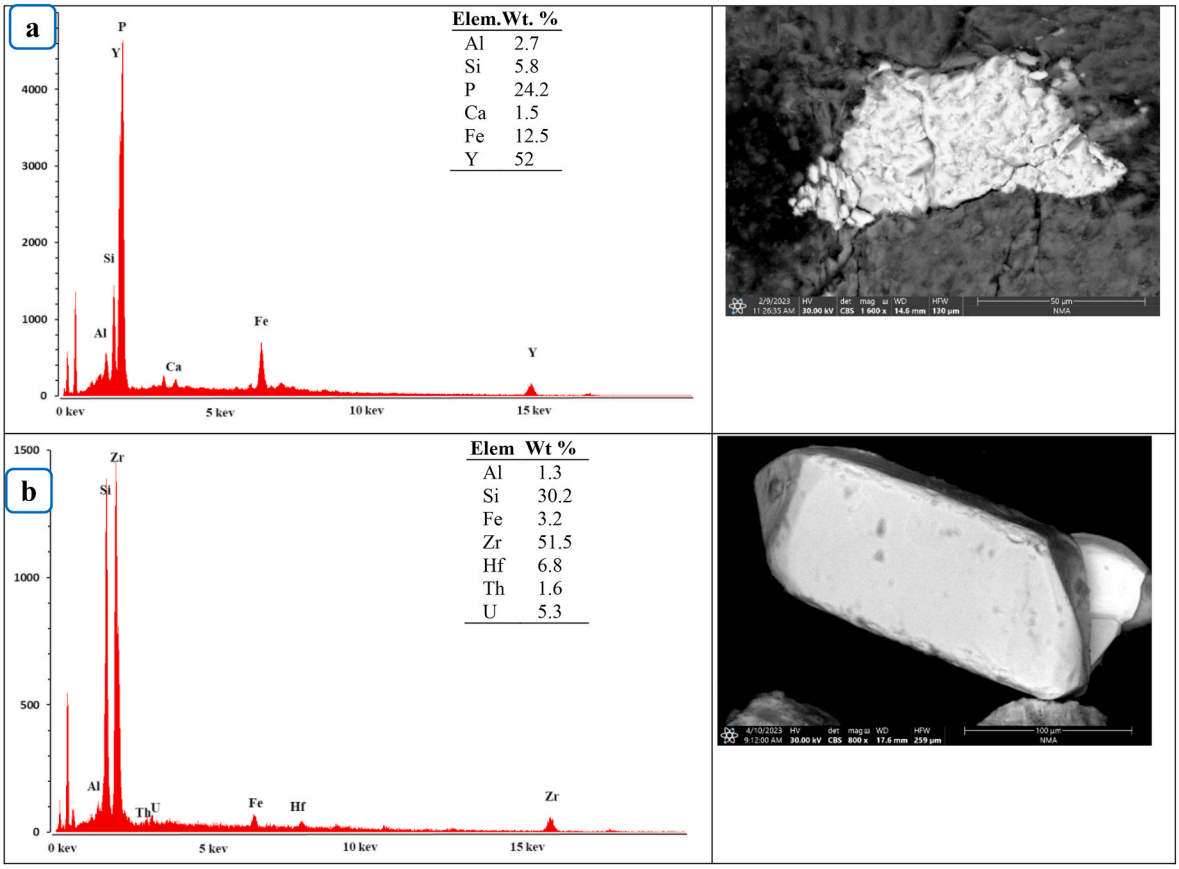

Fig. 6. EDX spectra and BSE image of: **a**) Xenotime and **b**) Zircon mineral.

in various mineral references [59,60]. Tantite forms transparent microscopic colorless, triclinic crystals with an adamantine luster. Chemical analyses show Ta (85.7 wt%) with traces of Si and Al (Fig. 5c).

D. Accessory minerals

Xenotime (YPO_4) is a rare mineral which occurs, like monazite, as an accessory constituent in granites and crystalline metamorphic rocks. Xenotime mineral appear in reddish brown, translucent to opaque. The EDX reveals that it consists of Y (52 wt%) and P (24.2 wt%) with traces of Ca and Fe (Fig. 6a).

Zircon crystals are euhedral, with six to eight sides. Some of the analyzed zircon grains exhibit lengthening, indicating that a high fluid supply induces the time of zircon crystallization to prolong. Isolated euhedral to subhedral zircon crystals is confirmed by EDX analyses (Fig. 6b).

E. Precious and Base Metals

Gold (Au) is the main precious minerals that recorded in the studied samples. Gold is present as specks with high concentration (48.9 wt %) blended with silica and copper (Fig. 7a). Argentite (Ag_2S) refers to the high temperature form of silver sulphide.

Argentite is a relatively rare Ag ore found in hydrothermal veins (silver sulfide high temperature, which is stable over 177 °C), primarily in the alteration zone. Below 177 °C is transformed to acanthite. It has been linked with pyrite, sphalerite, and galena. It is also a mineral accompanied by gold in the epithermal veins. The EDX analysis give an Ag (85.5–70.9 wt %), S (7.5–3.1) (Fig. 7b–c). Some grains was found as inclusion on zircon (Fig. 8a).

Cassiterite (SnO_2) is a basic metal in the rutile group. It can be identified in hydrothermal veins with temperatures ranging from low to high. EDX analysis revealed the presence of Sn (71.5 wt %), and O (28.5 wt%) contents (Fig. 8b).

Wolframite (Fe, Mn) is midway between ferberite (Fe^{2+}-rich) and hübnerite (Mn^{2+}-rich) which is the primary resource of tungsten. It has been identified and verified by ESEM that it contained W (47.2 wt%), Fe (7.2 wt%), and Mn (10 wt%) (Fig. 8c).

Galena is mostly composed of lead sulfide (PbS) with trace metals such as Fe and calcium. The ESEM approach revealed the presence of Pb (79.9 wt%) and S (14.9 wt%) (Fig. 9a). (Fig. 9a).

Mimetite $Pb_5(AsO_4)_3Cl$ is member of apatite group. This mineral was recorded having a chemical composition of Pb (69.6 wt %), As (13.8 wt %) and Cl (2.3 wt %) (Fig. 9b). cotunnite)$PbCl_2$) crystals are differentiated by orthorhombic coherence, which explains the possible anisotropy of chloride ionic mobility in these crystals. It develops at temperatures less than 325 °C. Its grain ranged from anhedral to subhedral, with rounded to subrounded surfaces. The EDX examination of cotunnite mineral grains indicates that they are primarily constituted of Pb (75.5 wt%) and Cl (24 wt%).

5. Discussion

5.1. Statistical analysis

The statistical parameters, including the mean, standard deviation, min., max., and quartile values of ^{232}Th, ^{238}U, and ^{40}K concentrations across the study area, offer insightful information about their distribution and their effects on the environment (Table 1).

^{232}Th concentrations exhibit the lowest mean value among the three activity concentrations, with smaller standard deviation for the different rock units. Its concentration ranges from 40.40 $Bqkg^{-1}$ (in monzogranites) to 424.20 $Bqkg^{-1}$ (in the altered granites), reflecting moderate heterogeneity in thorium distribution in comparison to ^{238}U, and

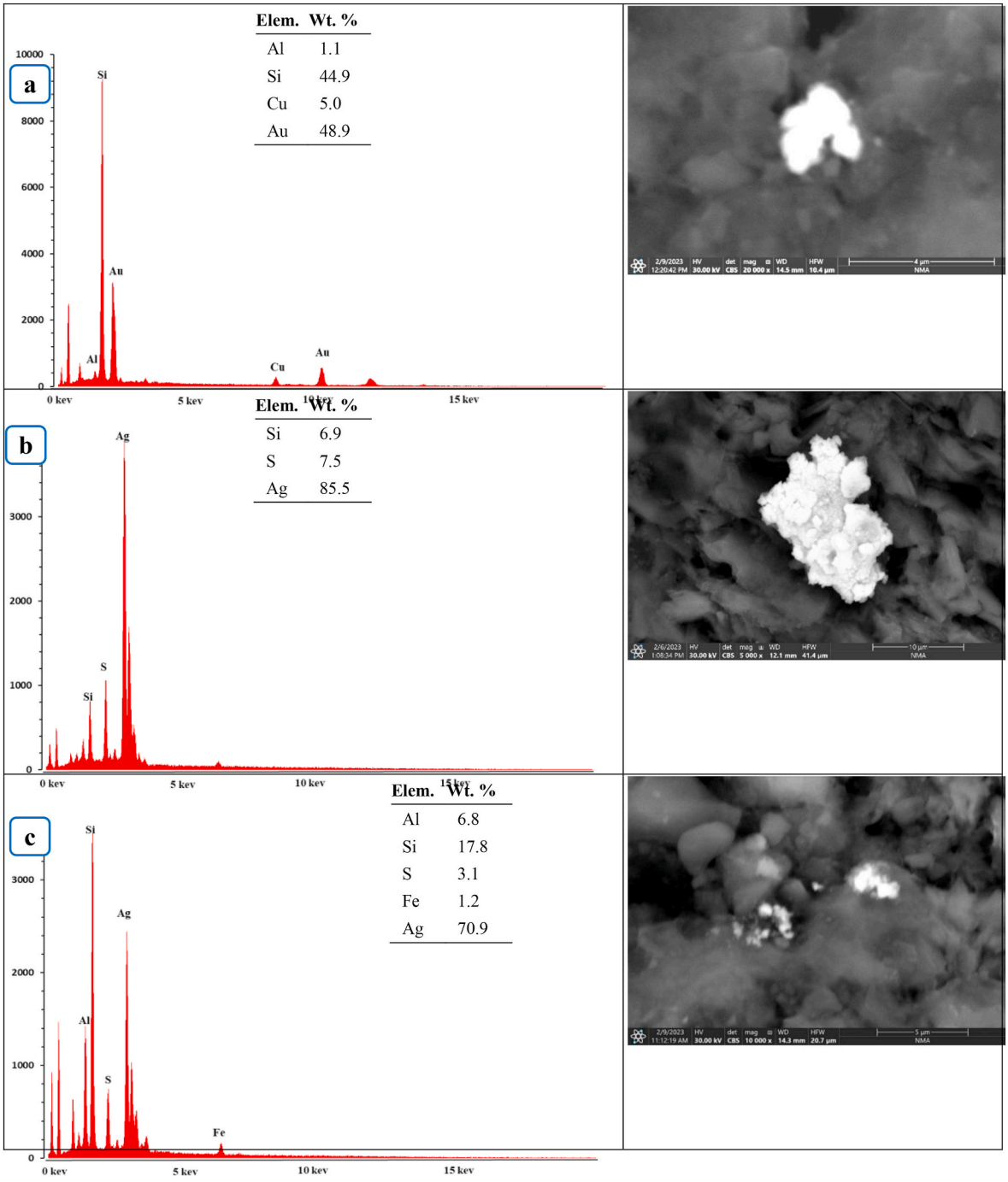

Fig. 7. EDX spectra and BSE image of: **a**) gold and **b-c**) argentite.

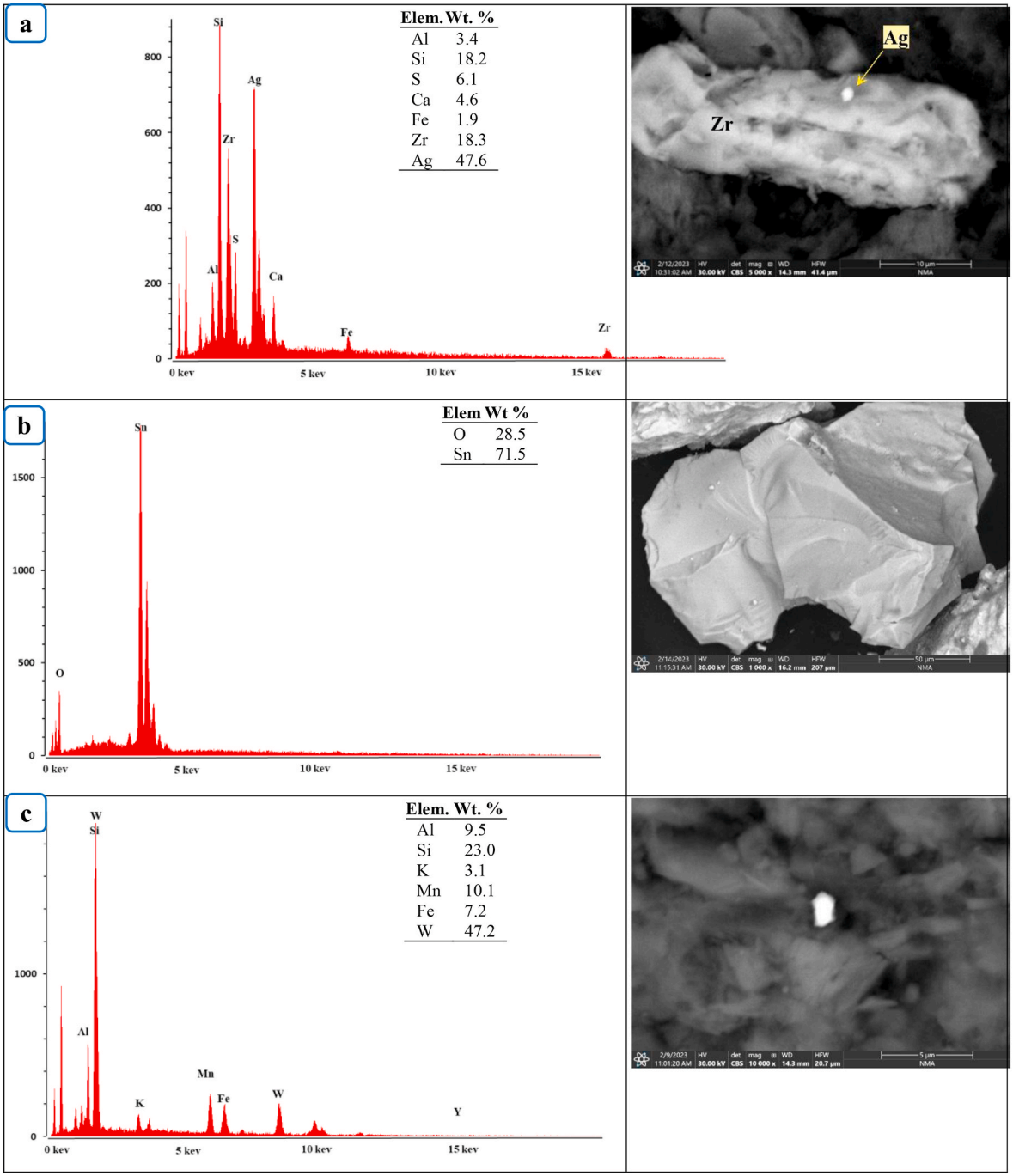

Fig. 8. EDX spectra and BSE image of: **a**) Argentite, b) Cassiterite, and c) Wolframite mineral.

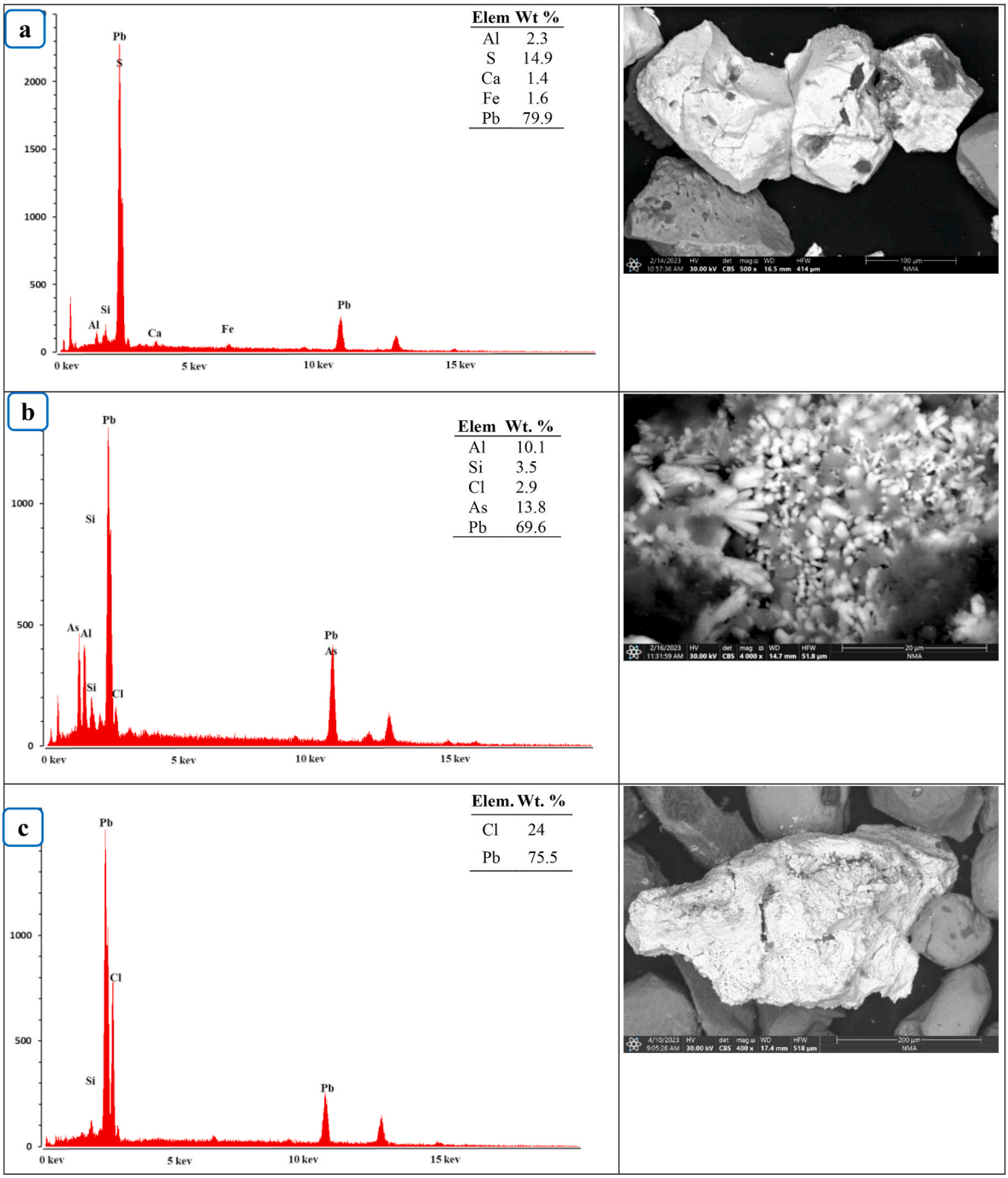

Fig. 9. EDX spectra and BSE image of a) Galena, d) Mimetite, and c) Cotunnite mineral.

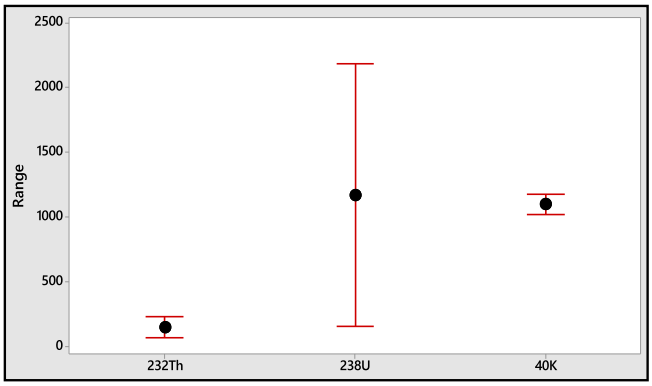

Fig. 10. Interval plot of: a) ^{232}Th, b) ^{238}U, and c) ^{40}K concentrations.

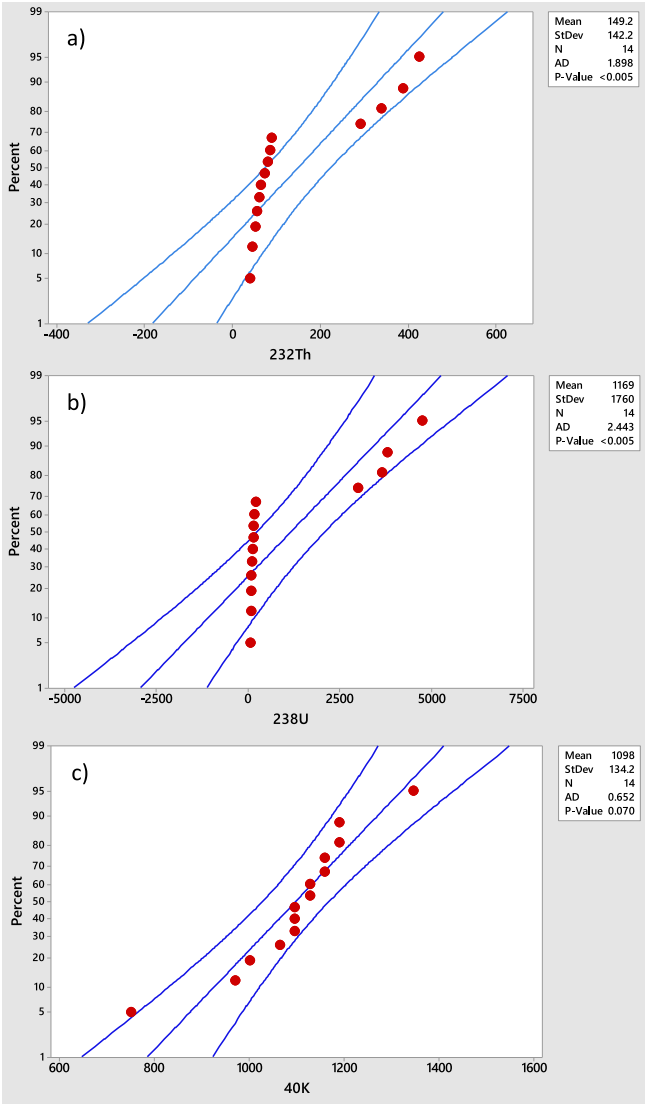

Fig. 11. Distribution probability of: a) ^{232}Th, b) ^{238}U, and c) ^{40}K.

^{40}K concentrations (Fig. 10). The interquartile range (57.57–240.38 Bqkg^{-1}) points to that most samples have different thorium levels with clear variations. However, the average concentration of ^{238}U is 1169.143 Bqkg^{-1}, with a high standard deviation of 1760.36 Bqkg^{-1}, indicating high variability in the examined rocks. The lowest recorded concentration is 89.28 Bqkg^{-1} (in monzogranites), while the highest reaches 3797.5 Bqkg^{-1} (in the altered granites). The median value (1169.143 Bqkg^{-1}) and interquartile range (89.9–2290.9 Bqkg^{-1}) points to that most samples have relatively wide uranium variations. Moreover, the mean concentration of ^{40}K is 1097.74 Bqkg^{-1}, with a standard deviation (134.18 Bqkg^{-1}), indicating substantial variation in potassium levels across the rock units. The concentration ranges from a minimum of 751.2 Bqkg^{-1} (in monzogranites) to a maximum of 1345.9 Bqkg^{-1} (in the altered granites), suggesting that the altered granites have significantly higher levels, likely referring to their content of radioactive minerals. The interquartile range (IQR: 1072–1158 Bqkg^{-1}) further highlights limited variability.

A popular statistical technique for figuring out whether a dataset has a normal distribution is the Shapiro-Wilk test [61]. The results of the Shapiro-Wilk test are corroborated by the normal probability maps in Fig. 11. The ^{238}U and ^{232}Th points show a non-normal distribution, as they diverge from a straight line. The ^{40}K data points resemble a nearly straight line, indicating that these characteristics have a normal distribution. Table 3 reveals the Pearson correlation of radioactive measurements in the Magal Gebreel rocks, which indicates the level of collaboration among the radioactive constituents. Tanasković [62] state that the correlation frequency was divided into four main categories: very strong (0.8–1.0), moderate (0.2–0.39), high (0.4–0.79), and weak (0.00–0.19). According to the contour map (Fig. 12), Table 3 demonstrates a very strong positive correlation between ^{232}Th and ^{238}U (R2 = 0.995). This table indicates a moderate correlation between ^{232}Th and ^{40}K activity compared to ^{238}U. This is explained by the concurrent occurrence of these radioactive substances in nature. Additionally, there is a significant and positive correlation between ^{238}U and ^{232}Th and the radiological risk indicators. This is because radiological factors are linked to radionuclides, which are known to be primarily gamma-ray generating elements in nature [63].

5.2. Radiation risk impact

The radioactivity of the Magal Gebreel rocks has been assessed using a range of indicators, encompassing D_{air}, $AED_{out\&in}$, ELCR, D_{organ}, and Raeq. Furthermore, further parameters have been stated, such as H_{ex} and H_{in} (Table 4).

As stated by Kumar [64] the D_{air} aspect is employed for assessing the frequency of radiation that survives from the exterior of the Earth over a meter. The tested samples had D_{air} measurements ranging from 93.14 ± 19.50 (in monzogranites) to 2374.63 ± 346.49 (in altered granites) nGy/h, which surpass the international average of 59 nGy/h [35,46,50,65–67]. It's obvious that the altered granites had the highest D_{air} values, ranging from 1535.27 to 2374.63 nGy/h, while the minimal is recorded in monzogranites (93.14–133.06 nGy/h). As a consequence, gamma ray irradiation modifies the R_{aeq} as well as its inside and outside alpha particles. The predicted mean amounts (R_{aeq}) for monzogranites (239.87 ± 42.13 Bqkg^{-1}) and alkali feldspar granites (343.52 ± 57.73 Bqkg^{-1}) fall within the permissible range of 370 Bqkg^{-1} [36,62]. In contrast, the R_{aeq} of the altered granite ranges from 3507.99 to 5447.39 Bqkg^{-1}, with an average of 4405.30 ± 800.37 Bqkg^{-1}, surpassing the permissible amount [35,65,66]. The D_{air} findings, conversion number (0.7 SvGy^{-1}), and outdoor (0.2) and indoor (0.8) occupation coefficients are employed for estimating the yearly radiation applying both the indoor (AED_{in}) and outdoor (AED_{out}) attitudes. All of the samples evaluated had AED_{out} readings that varied between 0.11 and 2.91 mSvy^{-1}, surpassing the allowable limit of 0.07 mSvy^{-1} [18,37,41,43]. The altered granites have a higher mean AED_{out} (2.36 ± 0.42 mSvy^{-1}) than typical Magal Gebreel rocks. Likewise to AED_{out}, altered granites have the greatest average AED_{in} value (9.44 ± 1.7 mSvy^{-1}). Furthermore, all of the tested rocks have AED_{in} concentrations over the permitted level [35].

The amount of radioactivity that has accumulated in the tissue of an individual can be determined via the human organ dosage (indoor and outdoor) efficient dosages (D_{organ}), and conversions factor like 0.58, 0.64, 0.46, 0.69, 0.82, 0.62, and 0.68 can be obtained for specific organs

Table 3
Pearson's correlation of the activity concentrations and hazard parameters.

	^{232}Th	^{238}U	^{40}K	D_{air}	H_{in}	H_{ex}	AED_{out}	AED_{in}	R_{aeq}
^{238}U	0.995								
^{40}K	0.470	0.446							
D_{air}	0.996	1.000	0.454						
H_{in}	0.995	1.000	0.449	1.000					
H_{ex}	0.996	1.000	0.452	1.000	1.000				
AED_{out}	0.996	1.000	0.455	1.000	1.000	1.000			
AED_{in}	0.996	1.000	0.454	1.000	1.000	1.000	1.000		
R_{aeq}	0.996	1.000	0.453	1.000	1.000	1.000	1.000	1.000	
ELCR	0.996	1.000	0.454	1.000	1.000	1.000	1.000	1.000	1.000

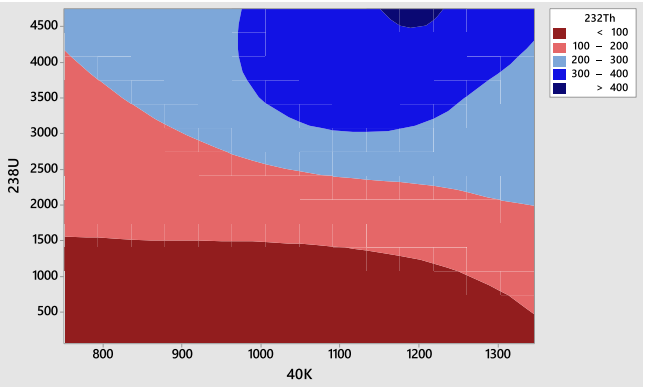

Fig. 12. Color map of ^{232}Th vs. ^{238}U and ^{40}K for the assessed rocks.

like the ovaries, lung, liver, bone marrow, testes, kidneys, and entire body [37]. It is clear that both the outdoor ($D_{organout}$) and indoor ($D_{organin}$) readings are less than one (acceptable limits), with the indoor values exceeding the outdoor readings for the analyzed monzogranites and alkali feldspar granites. Additionally, contrasted to other human tissues, the liver obtains least amount of radiation both indoors and outdoors (D_{organ}), while the testes obtain the most exposure (Table 4). The altered rocks have the greatest D_{organs} values, which surpass the allowable norms [35]. Furthermore, the projected $D_{organin}$ values are higher than $D_{organout}$ for all rock units, specifically altered rocks.

The H_{in} and H_{ex} parameters may be employed to evaluate radiation's influence on people [35,68,69]. The computed mean values of H_{in} and H_{ex} for monzogranite are 0.89 ± 0.17 and 0.65 ± 0.11, respectively, which are below the permissible limit. Alternatively, the alkali feldspar granites (with 1.32 ± 0.28 for H_{in} and 0.93 ± 0.16 for H_{ex}) and altered granites with high levels of H_{in} (22.17 ± 4.12) and H_{ex} (11.90 ± 2.16) pose considerable dangers to health, suggesting there are serious health hazards associated with these samples [3,34,65,66,69,70].

The mean ELCR values of all the studied samples (0.49 ± 0.08 × 10^{-3} for monzogranites (Table 3), 0.69 ± 0.11 × 10^{-3} for alkali feldspar granites, and 8.26 ± 1.49 × 10^{-3} for altered granites) exceed the permitted range of 0.029 × 10^{-3} [13]. This suggests that a person can develop cancer after a lifetime of intimate contact with examined rocks. As previously stated, the radiological hazard characteristics of the gathered samples exhibit a sequence (from low to high risk): monzogranites progress to alkali feldspar granites and then altered granites.

6. Conclusions

The Magal Gebreel rocks, which include monzogranites, alkali feldspar granites, and altered granites, have been tested for proportional radioactive distribution and mineralization. The altered granites have the greatest acquired activity concentrations of ^{232}Th (290.88–424.20 Bqkg^{-1}), ^{40}K (1095.50–1345.90 Bqkg^{-1}), and ^{238}U (2988.40–4749.20 Bqkg^{-1}), and their total (^{238}U + ^{40}K + ^{232}Th = avg. 2201.60 ± 250.62 Bqkg^{-1}), contingent upon NaI detector findings. This is due to the presence of radioactive minerals such as kasolite, uranophane, allanite, zircon, and thorite, which integrate radionuclides into their structure. Radiological indicators such as absorbed dose rate, excess life-time cancer, annualized dosage, dose to human organs, radium equivalent, and other factors have been predicted for these rocks. The bulk of factors readings are greater than the global median, indicating that natural gamma radiation generated has a considerable influence, most likely from altered granites. Microscopic inspection and ESEM analysis revealed significant mineral assemblages within the Magal Gebreel rocks, including precious and base metals, accessory, radioactive-bearing, REE-bearing, and Nb-Ta-bearing minerals.

CRediT authorship contribution statement

Gehad M. Saleh: Writing – review & editing, Methodology, Formal analysis, Conceptualization. **Basma A. El-Badry:** Writing – review & editing, Supervision, Software, Formal analysis. **Mabrouk Sami:** Writing – review & editing, Validation, Investigation. **Tamader Alhazani:** Supervision, Validation, Writing – review & editing. **Omnia T. Amer:** Writing – review & editing, Software, Methodology. **Ioan V. Sanislav:** Writing – review & editing, Supervision, Investigation. **El Saeed R. Lasheen:** Writing – review & editing, Writing – original draft, Software, Investigation, Data curation, Conceptualization.

Availability of data and material

Each component of data that was evaluated throughout this research is included in this paper.

Ethical approval

No research with human beings has been carried out by any of the authors of this paper.

Funding

This work was supported and funded by the Deanship of Scientific

Table 4
Radiological parameters of the Magal Gebreel rocks.

Rocks	Samples	Dair nGy/h	H_{in}	H_{ex}	AED_{out} (mSv/y)	AED_{in} (mSv/y)	R_{aeq}	ELCR	Dorgans out (mSv/y)							Dorgans in (mSv/y)						
									Liver	Ovaries	Kidneys	Lungs	Bone Marrow	Testes	Entire Body	Liver	Ovaries	Kidneys	Lungs	Bone Marrow	Testes	Entire Body
Monzogranites	**MG1**	93.14	0.73	0.53	0.11	0.46	195.79	0.40	0.05	0.07	0.07	0.07	0.08	0.09	0.08	0.21	0.27	0.28	0.29	0.32	0.37	0.32
	MG2	122.26	0.92	0.68	0.15	0.60	253.49	0.52	0.07	0.09	0.09	0.10	0.10	0.12	0.10	0.28	0.35	0.37	0.38	0.41	0.49	0.41
	MG3	133.06	1.10	0.76	0.16	0.65	282.00	0.57	0.08	0.09	0.10	0.10	0.11	0.13	0.11	0.30	0.38	0.40	0.42	0.45	0.54	0.45
	MG4	130.40	1.01	0.74	0.16	0.64	273.58	0.56	0.07	0.09	0.10	0.10	0.11	0.13	0.11	0.29	0.37	0.40	0.41	0.44	0.52	0.44
	MG5	94.32	0.69	0.53	0.12	0.46	194.49	0.40	0.05	0.07	0.07	0.07	0.08	0.09	0.08	0.21	0.27	0.29	0.30	0.32	0.38	0.32
	Min.	93.14	0.69	0.53	0.11	0.46	194.49	0.40	0.05	0.07	0.07	0.07	0.08	0.09	0.08	0.21	0.27	0.28	0.29	0.32	0.37	0.32
	Max.	133.06	1.10	0.76	0.16	0.65	282.00	0.57	0.08	0.09	0.10	0.10	0.11	0.13	0.11	0.30	0.38	0.40	0.42	0.45	0.54	0.45
	Avg.	114.63	0.89	0.65	0.14	0.56	239.87	0.49	0.06	0.08	0.09	0.09	0.10	0.12	0.10	0.26	0.33	0.35	0.36	0.39	0.46	0.39
	SD	19.50	0.17	0.11	0.02	0.10	42.13	0.08	0.01	0.01	0.01	0.02	0.02	0.02	0.02	0.04	0.06	0.06	0.06	0.07	0.08	0.07
Alkali feldspar granites	**MG6**	118.36	0.86	0.66	0.15	0.58	245.41	0.51	0.07	0.08	0.09	0.09	0.10	0.12	0.10	0.27	0.34	0.36	0.37	0.40	0.48	0.40
	MG7	181.07	1.59	1.05	0.22	0.89	389.15	0.78	0.10	0.13	0.14	0.14	0.15	0.18	0.15	0.41	0.52	0.55	0.57	0.61	0.73	0.61
	MG8	177.10	1.49	1.02	0.22	0.87	378.32	0.76	0.10	0.13	0.13	0.14	0.15	0.18	0.15	0.40	0.50	0.54	0.56	0.60	0.71	0.60
	MG9	170.50	1.38	0.98	0.21	0.84	362.66	0.73	0.10	0.12	0.13	0.13	0.14	0.17	0.14	0.38	0.49	0.52	0.54	0.58	0.69	0.58
	MG10	161.17	1.29	0.92	0.20	0.79	342.07	0.69	0.09	0.11	0.12	0.13	0.14	0.16	0.13	0.36	0.46	0.49	0.51	0.55	0.65	0.55
	Min.	118.36	0.86	0.66	0.15	0.58	245.41	0.51	0.07	0.08	0.09	0.09	0.10	0.12	0.10	0.27	0.34	0.36	0.37	0.40	0.48	0.40
	Max.	181.07	1.59	1.05	0.22	0.89	389.15	0.78	0.10	0.13	0.14	0.14	0.15	0.18	0.15	0.41	0.52	0.55	0.57	0.61	0.73	0.61
	Avg.	161.64	1.32	0.93	0.20	0.79	343.52	0.69	0.09	0.11	0.12	0.13	0.14	0.16	0.13	0.36	0.46	0.49	0.51	0.55	0.65	0.55
	SD	25.34	0.28	0.16	0.03	0.12	57.63	0.11	0.01	0.02	0.02	0.02	0.02	0.03	0.02	0.06	0.07	0.08	0.08	0.09	0.10	0.09
Altered granites	**MG11**	1847.59	21.32	11.44	2.27	9.06	4232.46	7.93	1.04	1.31	1.40	1.45	1.56	1.86	1.54	4.17	5.26	5.62	5.80	6.25	7.43	6.25
	MG12	1935.90	22.24	11.98	2.37	9.50	4433.36	8.31	1.09	1.38	1.47	1.52	1.64	1.95	1.61	4.37	5.51	5.89	6.08	6.55	7.79	6.55
	MG13	1535.27	17.56	9.48	1.88	7.53	3507.99	6.59	0.87	1.09	1.17	1.21	1.30	1.54	1.28	3.46	4.37	4.67	4.82	5.20	6.18	5.20
	MG14	2374.63	27.56	14.72	2.91	11.65	5447.39	10.19	1.34	1.69	1.81	1.86	2.01	2.39	1.98	5.36	6.76	7.22	7.46	8.04	9.55	8.04
	Min.	1535.27	17.56	9.48	1.88	7.53	3507.99	6.59	0.87	1.09	1.17	1.21	1.30	1.54	1.28	3.46	4.37	4.67	4.82	5.20	6.18	5.20
	Max.	2374.63	27.56	14.72	2.91	11.65	5447.39	10.19	1.34	1.69	1.81	1.86	2.01	2.39	1.98	5.36	6.76	7.22	7.46	8.04	9.55	8.04
	Avg.	1923.35	22.17	11.90	2.36	9.44	4405.30	8.26	1.09	1.37	1.46	1.51	1.63	1.93	1.60	4.34	5.47	5.85	6.04	6.51	7.74	6.51
	SD	346.49	4.12	2.16	0.42	1.70	800.37	1.49	0.20	0.25	0.26	0.27	0.29	0.35	0.29	0.78	0.99	1.05	1.09	1.17	1.39	1.17

Research at Imam Mohammad Ibn Saud Islamic University (IMSIU) (grant number IMSIU-DDRSP2602).

Declaration of competing interest

The authors declare that they have no known competing financial interests or personal relationships that could have appeared to influence the work reported in this paper.

Appendix A. Supplementary data

Supplementary data to this article can be found online at https://doi.org/10.1016/j.net.2026.104165.

References

[1] I. Akkurt, K. Günoğlu, Natural radioactivity measurements and radiation dose estimation in some sedimentary rock samples in Turkey, Sci. Technol. Nucl. Install. 2014 (2014) 1–6, https://doi.org/10.1155/2014/950978.

[2] B.A. Al-Mur, M.H. Aljahdali, T. Almeelbi, E.S.R. Lasheen, Spatial radionuclide distribution, mineralogy, and radiological evaluation of the Jeddah shoreline sediments, Red Sea, Saudi Arabia, Environ. Monit. Assess. 197 (2025) 593, https://doi.org/10.1007/s10661-025-13986-8.

[3] S. Özden, S.A. Pehlivanoğlu, O. Günay, Evaluation of natural radioactivity in soils of Konya (Turkey) and estimation of radiological health hazards, Environ. Monit. Assess. 195 (2023) 1523, https://doi.org/10.1007/s10661-023-12162-0.

[4] S. Özden, S. Aközcan, Natural radioactivity measurements and evaluation of radiological hazards in sediment of Aliağa Bay, İzmir (Turkey), Arabian J. Geosci. 14 (2021) 64, https://doi.org/10.1007/s12517-020-06446-9.

[5] R.C. Ramola, V.M. Choubey, G. Prasad, G.S. Gusain, Z. Tosheva, A. Kies, Radionuclide analysisin the soil of Kumaun himalaya, India, using gamma ray spectrometry, Curr. Sci. 100 (2011) 6–25.

[6] B. Lei, L. Zhao, F. Girault, Z. Cai, C. Luo, S. Thapa, J. She, F. Perrier, Overview and large-scale representative estimate of radon-222 flux data in China, Environ. Adv. 11 (2023) 100312, https://doi.org/10.1016/j.envadv.2022.100312.

[7] M.Y. Krebs, D.G. Pearson, A.J. Fagan, Y. Bussweiler, C. Sarkar, The application of trace elements and Sr–Pb isotopes to dating and tracing ruby formation: the aappaluttoq deposit, SW Greenland, Chem. Geol. 523 (2019) 42–58, https://doi.org/10.1016/j.chemgeo.2019.05.035.

[8] G.M. Saleh, E.S.R. Lasheen, M. Foi, F. Abdalla, A. Abdelaal, Assessment of radioactivity and heavy metal pollution levels in the coastal sediments in the Red Sea region of Sharm El Luli, Egypt, Water. Air. Soil Pollut. 236 (2025) 319, https://doi.org/10.1007/s11270-025-07962-8.

[9] A.G.E. Abbady, M.A.M. Uosif, A. El-Taher, Natural radioactivity and dose assessment for phosphate rocks from Wadi El-Mashash and El-Mahamid mines, Egypt, J. Environ. Radioact. 84 (2005) 65–78, https://doi.org/10.1016/j.jenvrad.2005.04.003.

[10] B.A. Al-Mur, A. Gad, Radiation hazard from natural radioactivity in the marine sediment of Jeddah Coast, Red Sea, Saudi Arabia, J. Mar. Sci. Eng. 10 (2022) 1145, https://doi.org/10.3390/jmse10081145.

[11] D. Fathy, H.M.H. Zakaly, E.S.R. Lasheen, R. Elsaman, S.S. Alarifi, M. Sami, H. A. Awad, A. Ene, Assessing geochemical and natural radioactivity impacts of hamadat phosphatic mine through radiological indices, PLoS One 18 (2023) e0287422, https://doi.org/10.1371/journal.pone.0287422.

[12] H. Li, Q. Wang, C. Zhang, W. Su, Y. Ma, Q. Zhong, E. Xiao, F. Xia, G. Zheng, T. Xiao, Geochemical distribution and environmental risks of radionuclides in soils and sediments runoff of a uranium mining area in south China, Toxics 12 (2024) 95, https://doi.org/10.3390/toxics12010095.

[13] A.A. Qureshi, S. Tariq, K.U. Din, S. Manzoor, C. Calligaris, A. Waheed, Evaluation of excessive lifetime cancer risk due to natural radioactivity in the rivers sediments of Northern Pakistan, J. Radiat. Res. Appl. Sci. 7 (2014) 438–447, https://doi.org/10.1016/j.jrras.2014.07.008.

[14] T. Raghavendra, K. Vishwaprasad, G. Kalyani, T. Vijayalakshmi, V. Himabindu, J. Arunachalam, P. Padmasavithri, V. Kumar, R.M. Tripathi, Assessment of natural radioactivity in soils around the proposed uranium mining site of lambapur – peddagattu and seripally, India, J. Geol. Soc. India 93 (2019) 223–227, https://doi.org/10.1007/s12594-019-1156-2.

[15] I.F. Al-Hamarneh, M.I. Awadallah, Soil radioactivity levels and radiation hazard assessment in the highlands of northern Jordan, Radiat. Meas. 44 (2009) 102–110, https://doi.org/10.1016/j.radmeas.2008.11.005.

[16] J.H. AlZahrani, W.R. Alharbi, A.G.E. Abbady, Radiological impacts of natural radioactivity and heat generation by radioactive decay of phosphorite deposits from northwestern Saudi Arabia, Aust. J. Basic Appl. Sci. 5 (2011) 683–690.

[17] F.M. Khaleal, M.A. Tahoon, G.M. Saleh, M.S. Kamar, H.M.H. Zakaly, I.H. Zidan, B. A. Al-Mur, S.S. Alarif, E.S.R. Lasheen, Dolphin-shaped island: exploring the natural resources and radiological hazards of Wadi El Gemal Island, Mar. Pollut. Bull. 194 (2023) 115367, https://doi.org/10.1016/j.marpolbul.2023.115367.

[18] R. Ravisankar, J. Chandramohan, A. Chandrasekaran, J. Prince Prakash Jebakumar, I. Vijayalakshmi, P. Vijayagopal, B. Venkatraman, Assessments of radioactivity concentration of natural radionuclides and radiological hazard indices in sediment samples from the East coast of Tamilnadu, India with statistical approach, Mar. Pollut. Bull. 97 (2015) 419–430, https://doi.org/10.1016/j.marpolbul.2015.05.058.

[19] S.K. Sahoo, M. Hosoda, S. Kamagata, A. Sorimachi, T. Ishikawa, S. Tokonami, S. Uchida, Thorium, uranium and rare Earth elements concentration in weathered Japanese soil samples, Prog. Nucl. Sci. Technol. 1 (2011) 416–419, https://doi.org/10.15669/pnst.1.416.

[20] W. Shehzad, K.H. Satti, M. Khan, K. Khan, A. Naseem, S. Ur Rehman, A. Jabbar, Estimation of background radiation levels and associated health risks in mineral rich district Chiniot, Pakistan, J. Radioanal. Nucl. Chem. 319 (2019) 1051–1058, https://doi.org/10.1007/s10967-019-06425-9.

[21] I. Vukasinovic, A. Djordjevic, M. Rajkovic, D. Todorovic, V. Pavlovic, Distribution of natural radionuclides in anthrosol-type soil, Turk. J. Agric. For. (2010), https://doi.org/10.3906/tar-0911-59.

[22] P. Sola, W. Srinuttrakul, S. Laoharojanaphand, N. Suwankot, Estimation of indoor radon and the annual effective dose from building materials by ionization chamber measurement, J. Radioanal. Nucl. Chem. 302 (2014) 1531–1535, https://doi.org/10.1007/s10967-014-3716-7.

[23] L. Vimercati, F. Fucilli, D. Cavone, L. De Maria, F. Birtolo, G. Ferri, L. Soleo, P. Lovreglio, Radon levels in indoor environments of the university hospital in bari-apulia region Southern Italy, Int. J. Environ. Res. Publ. Health 15 (2018) 694, https://doi.org/10.3390/ijerph15040694.

[24] P. Kuzmanović, N. Todorović, J. Nikolov, J. Hansman, A. Vraničar, J. Knežević, B. Miljević, Assessment of radiation risk and radon exhalation rate for granite used in the construction industry, J. Radioanal. Nucl. Chem. 321 (2019) 565–577, https://doi.org/10.1007/s10967-019-06592-9.

[25] E.S.R. Lasheen, G.M. Saleh, A. El-Tohamy, F.M. Khaleal, M. Sami, I.V. Sanislav, F. Abdalla, Mineral chemistry and whole-rock analysis of Magnesian and ferroan granitic suites of magal gebreel, south eastern desert: clues for Neoproterozoic Syn- and post-collisional felsic magmatism, Minerals 15 (2025) 751, https://doi.org/10.3390/min15070751.

[26] G.M. Saleh, M.S. Kamar, F.M. Khaleal, M.K. Azer, T. Nasr, E.S.R. Lasheen, Petrogenesis and tectonic evolution of tourmaline- bearing leucogranites, Sikait area, Southeastn desert of Egypt utilizing mineralogical and bulk rock analysis, Sci. Rep. 15 (2025) 20191, https://doi.org/10.1038/s41598-025-06155-x.

[27] E.S.R. Lasheen, M. Sami, A.A. Hegazy, H. Arman, I.V. Sanislav, M.S. Ahmed, M. A. Rashwan, Petrological characteristics and physico-mechanical properties of dokhan volcanics for decorative stones and building material applications, Buildings 14 (2024) 3418, https://doi.org/10.3390/buildings14113418.

[28] E.S.R. Lasheen, M.A. Rashwan, M.K. Azer, Effect of mineralogical variations on physico-mechanical and thermal properties of granitic rocks, Sci. Rep. 13 (2023) 10320, https://doi.org/10.1038/s41598-023-36459-9.

[29] M.Z. El-Bialy, H.A. Eliwa, N.M. Mahdy, M. Murata, K.H. El-Gameel, H. Sehsah, M. Omar, Y. Kato, K. Fujinaga, A. Andresen, T.B. Thomsen, U-Pb zircon geochronology and geochemical constraints on the Ediacaran continental arc and post-collision granites of Wadi Hawashiya, North Eastern desert, Egypt: insights into the ~600 Ma crust-forming event in the northernmost part of Arabian-Nubian shield, Precambr. Res. 345 (2020) 105777, https://doi.org/10.1016/j.precamres.2020.105777.

[30] B. Jahn, F. Wu, R. Capdevila, F. Martineau, Z. Zhao, Y. Wang, Highly evolved juvenile granites with tetrad REE patterns: the Woduhe and Baerzhe granites from the great Xing'an Mountains in NE China, Lithos 59 (2001) 171–198, https://doi.org/10.1016/S0024-4937(01)00066-4.

[31] M. Khan, H. Li, T.J. Algeo, A. Khan, M.W. Förster, Z. Ullah, Geochemistry and geochronology of a-type intermediate-felsic rocks in NW himalaya, Pakistan: implications for petrogenesis and tectonic evolution of Northern Gondwana, G-cubed 26 (2025), https://doi.org/10.1029/2024GC011802 e2024GC011802.

[32] E.S.R. Lasheen, R. Abart, M.S. Ahmed, K.M. Abdelfadil, E.S. Farahat, M. Sami, Petrological constraints of the Ediacaran magmatic intrusions, Homrit Mukpid area, southeastern desert, Egypt: bulk rock geochemistry and mineralogy, J. Afr. Earth Sci. 225 (2025) 105567, https://doi.org/10.1016/j.jafrearsci.2025.105567.

[33] F. Wu, D. Sun, H. Li, B. Jahn, S. Wilde, A-type granites in northeastern China: age and geochemical constraints on their petrogenesis, Chem. Geol. 187 (2002) 143–173, https://doi.org/10.1016/S0009-2541(02)00018-9.

[34] European Commission, Radiological protection principles concerning the natural radioactivity of building materials. Radiation Protection 112, Directorate General Environment. Nuclear Safety and Civil Protection, European Commission, 1999.

[35] UNSCEAR, in: Sources and Effects of Ionizing Radiation: United Nations Scientific Committee on the Effects of Atomic Radiation: UNSCEAR 2008 Report to the General Assembly, with Scientific Annexes, 2010. United Nations, New York.

[36] K.N. Yu, E.C.M. Young, M.J. Stokes, D.L. Luo, C.X. Zhang, Indoor radon and environmental gamma radiation in Hong Kong, Radiat. Protect. Dosim. 40 (1992) 259–263, https://doi.org/10.1093/oxfordjournals.rpd.a081212.

[37] K. O'Brien, R. Sanna, The distribution of absorbed dose-rates in humans from exposure to environmental gamma rays, Health Phys. (1976).

[38] S. Pavlidou, A. Koroneos, C. Papastefanou, G. Christofides, S. Stoulos, M. Vavelides, Natural radioactivity of granites used as building materials, J. Environ. Radioact. 89 (2006) 48–60, https://doi.org/10.1016/j.jenvrad.2006.03.005.

[39] H.M.H. Zakaly, H.A. Awad, E.S.R. Lasheen, S.A.M. Issa, R. Elsaman, M. U. Khandaker, H. Al-awah, D. Fathy, M. Sami, Radiometric and petrographic characterization of El-Yatima granite: evaluating radiological risks and mineralogical features, Radiat. Phys. Chem. 224 (2024) 111992, https://doi.org/10.1016/j.radphyschem.2024.111992.

[40] A.C. Freitas, A.S. Alencar, Gamma dose rates and distribution of natural radionuclides in sand beaches—Ilha grande, Southeastern Brazil, J. Environ. Radioact. 75 (2004) 211–223, https://doi.org/10.1016/j.jenvrad.2004.01.002.

[41] S. Sivakumar, A. Chandrasekaran, G. Senthilkumar, M. Suresh Gandhi, R. Ravisankar, Determination of radioactivity levels and associated hazards of coastal sediment from south east coast of Tamil Nadu with statistical approach, Iran. J. Sci. Technol. Trans. Sci. 42 (2018) 601–614, https://doi.org/10.1007/s40995-017-0184-2.
[42] H. Taskin, M. Karavus, P. Ay, A. Topuzoglu, S. Hidiroglu, G. Karahan, Radionuclide concentrations in soil and lifetime cancer risk due to gamma radioactivity in Kirklareli, Turkey, J. Environ. Radioact. 100 (2009) 49–53, https://doi.org/10.1016/j.jenvrad.2008.10.012.
[43] UNSCEAR, in: Sources and Effects of Ionizing Radiation: United Nations Scientific Committee on the Effects of Atomic Radiation: UNSCEAR 2000 Report to the General Assembly, with Scientific Annexes, 2000. United Nations, New York.
[44] E.S.R. Lasheen, H.E. Semary, S.Z. Kamh, G.M. Saleh, Advanced remote sensing techniques for mapping lithological units and radioactive alteration in the Southern Eastern desert, Egypt: petrological and radiological hazards determination, Adv. Space Res. (2026), https://doi.org/10.1016/j.asr.2025.12.109. S0273117725015522.
[45] M.U. Khandaker, A. Mahmud, M.M.M. Siraz, M.S. Alam, J.M. Trishna, MdB. Rashid, F. Hussin, M.A. Kassim, H. Osman, Identification of elevated level background radiation areas, exposure scenarios and implications for public health and environmental safety in Malaysia: a comprehensive study, Radiat. Phys. Chem. 235 (2025) 112851, https://doi.org/10.1016/j.radphyschem.2025.112851.
[46] A. Abdelaal, G.M. Saleh, E.S.R. Lasheen, M. Sami, F.M. Khaleal, I.V. Sanislav, F. Abdalla, Heavy metals and radioactivity assessment of the coastal sediments at Abu Ghusun, Southern Red Sea, Egypt, J. Radiat. Res. Appl. Sci. 18 (2025) 101976, https://doi.org/10.1016/j.jrras.2025.101976.
[47] J.M. Sharaf, M.S. Hamideen, Measurement of natural radioactivity in Jordanian building materials and their contribution to the public indoor gamma dose rate, Appl. Radiat. Isot. 80 (2013) 61–66, https://doi.org/10.1016/j.apradiso.2013.06.016.
[48] G. Senthilkumar, Y. Raghu, S. Sivakumar, A. Chandrasekaran, D. Prem Anand, R. Ravisankar, Natural radioactivity measurement and evaluation of radiological hazards in some commercial flooring materials used in Thiruvannamalai, Tamilnadu, India, J. Radiat. Res. Appl. Sci. 7 (2014) 116–122, https://doi.org/10.1016/j.jrras.2013.12.009.
[49] J. Guillén, J.J. Tejado, A. Baeza, A. Salas, J.G. Muñoz-Muñoz, Environmental impact of a granite processing factory as source of naturally occurring radionuclides, Appl. Geochem. 47 (2014) 122–129, https://doi.org/10.1016/j.apgeochem.2014.06.001.
[50] E.S.R. Lasheen, B.A. El-Badry, W.H. Mohamed, G.A. Khouqeer, I.V. Sanislav, M. Sami, Radioactivity and aeromagnetic of magmatic suites, Arabian Nubian shield: petrological and health risk characteristics, J. Radiat. Res. Appl. Sci. 18 (2025) 101910, https://doi.org/10.1016/j.jrras.2025.101910.
[51] S.F. Abdul Sani, M.K. Muhamad Azim, A.A. Marzuki, M.U. Khandaker, K. S. Almugren, E. Daar, F.H. Alkallas, D.A. Bradley, Radioactivity and elemental concentrations of natural and commercial salt, Radiat. Phys. Chem. 190 (2022) 109790, https://doi.org/10.1016/j.radphyschem.2021.109790.
[52] A. Shahrokhi, M. Adelikhah, S. Chalupnik, E. Kocsis, E. Toth-Bodrogi, T. Kovács, Radioactivity of building materials in Mahallat, Iran – an area exposed to a high level of natural background radiation – attenuation of external radiation doses, Mater. Construcción 70 (2020) 233, https://doi.org/10.3989/mc.2020.03820.
[53] P. Kuzmanović, L. Filipović Petrović, J. Petrović, S. Forkapić, J. Hansman, D. Velimirović, J. Knežević Radić, Physico-chemical, technological and radiological characteristics of kaolinized granite from northwestern Serbia, Radiat. Phys. Chem. 222 (2024) 111885, https://doi.org/10.1016/j.radphyschem.2024.111885.
[54] R.M. Amin, Gamma radiation measurements of naturally occurring radioactive samples from commercial Egyptian granites, Environ. Earth Sci. 67 (2012) 771–775, https://doi.org/10.1007/s12665-012-1538-x.
[55] H.A. Awad, H.M.H. Zakaly, A.V. Nastavkin, A.M. El Tohamy, A. El-Taher, Radioactive mineralizations on granitic rocks and silica veins on shear zone of El-Missikat area, central Eastern Desert, Egypt, Appl. Radiat. Isot. 168 (2021), https://doi.org/10.1016/j.apradiso.2020.109493.
[56] A.M. El-Kammar, N. El-Hazik, M. Mahdi, N. Aly, Geochemistry of accessory minerals associated with radioactive mineralisation in the central Eastern desert, Egypt, J. Afr. Earth Sci. 25 (1997) 237–252, https://doi.org/10.1016/S0899-5362(97)00101-2.
[57] J. Hermann, Allanite: thorium and light rare earth element carrier in subducted crust, Chem. Geol. 192 (2002) 289–306, https://doi.org/10.1016/S0009-2541(02)00222-X.
[58] P. Černý, R. Chapman, K. Ferreira, S.-A. Smeds, Geochemistry of oxide minerals of Nb, Ta, Sn, and Sb in the Varuträsk granitic pegmatite, Sweden: the case of an "anomalous" columbite-tantalite trend, Am. Mineral. 89 (2004) 505–518, https://doi.org/10.2138/am-2004-0405.
[59] X.-D. Che, F.-Y. Wu, R.-C. Wang, A. Gerdes, W.-Q. Ji, Z.-H. Zhao, J.-H. Yang, Z.-Y. Zhu, In situ U–Pb isotopic dating of columbite–tantalite by LA–ICP–MS, Ore Geol. Rev. 65 (2015) 979–989, https://doi.org/10.1016/j.oregeorev.2014.07.008.
[60] T. Pan, Q.-F. Ding, X. Zhou, S.-P. Li, J. Han, L. Cheng, Columbite-Tantalite group mineral U-Pb geochronology of chaqiabeishan Li-Rich granitic pegmatites in the quanji massif, NW China: implications for the genesis and emplacement ages of pegmatites, Front. Earth Sci. 8 (2021) 606951, https://doi.org/10.3389/feart.2020.606951.
[61] A.S. Kanmi, U. Ibrahim, N.G. Goki, U. Rilwan, M.I. Sayyed, Y. Maghrbi, B.F. Namq, L.A. Najam, T.Y. Wais, Assessment of natural radioactivity and its radiological risks in the soil of local government areas (Asa, Ilorin East, Ilorin South, Irepodun, Moro, and Oyun) in Kwara state, Nigeria, Case Stud. Chem. Environ. Eng. 11 (2025) 101040, https://doi.org/10.1016/j.cscee.2024.101040.
[62] I. Tanasković, D. Golobocanin, N. Miljević, Multivariate statistical analysis of hydrochemical and radiological data of Serbian spa waters, J. Geochem. Explor. 112 (2012) 226–234, https://doi.org/10.1016/j.gexplo.2011.08.014.
[63] A.M.A. Adam, M.A.H. Eltayeb, Multivariate statistical analysis of radioactive variables in two phosphate ores from Sudan, J. Environ. Radioact. 107 (2012) 23–43, https://doi.org/10.1016/j.jenvrad.2011.11.021.
[64] N. Kumar, B. Khyalia, J. Yadav, B. Singh, V. Gupta, P.P. Singh, H. Singh, R. Dalal, Assessment of natural radioactivity in soil around Khetri copper belt of Rajasthan, India, J. Radioanal. Nucl. Chem. 333 (2024) 3185–3194, https://doi.org/10.1007/s10967-023-09301-9.
[65] R. Abd El Rahman, S. Taalab, Z. Al Full, M. Mohamed, M. Sayyed, N. Almousa, M. Hanfi, Natural radionuclide levels and radiological hazards of Khour abalea mineralized pegmatites, Southeastern desert, Egypt, Minerals 12 (2022) 353, https://doi.org/10.3390/min12030353.
[66] M.Y. Hanfi, A.E. Abdel Gawad, H. Eliwa, K. Ali, M.M. Taki, M.I. Sayyed, M. U. Khandaker, D.A. Bradley, Assessment of radioactivity in granitoids at nikeiba, Southeastern desert, Egypt; radionuclides concentrations and radiological hazard parameters, Radiat. Phys. Chem. 200 (2022) 110113, https://doi.org/10.1016/j.radphyschem.2022.110113.
[67] E.S.R. Lasheen, G.M. Saleh, B.A. Al-Mur, A. Abdelaal, Assessing the radioactive properties and environmental risks of hankorab sediments on the Red Sea coast, Environ. Earth Sci. 84 (2025) 420, https://doi.org/10.1007/s12665-025-12418-7.
[68] E.S.R. Lasheen, M.K. Azer, A. Ene, W. Abdelwahab, H.M.H. Zakaly, H.A. Awad, N. A. Kawady, Radiological hazards and natural radionuclide distribution in granitic rocks of Homrit Waggat Area, central Eastern desert, Egypt, Materials 15 (2022) 4069, https://doi.org/10.3390/ma15124069.
[69] A. Abbasi, H.M.H. Zakaly, F. Mirekhtiary, Baseline levels of natural radionuclides concentration in sediments east coastline of North Cyprus, Mar. Pollut. Bull. 161 (2020) 111793, https://doi.org/10.1016/j.marpolbul.2020.111793.
[70] M.F. Attallah, M.A. Hilal, Y.T. Mohamed, Preliminary investigations on reducing the high radiation risk level of TENORM scale waste from petroleum industry, Radiochim. Acta 106 (2018) 793–800, https://doi.org/10.1515/ract-2017-2904.